PERGAMON

Journal of Structural Geology 22 (2000) 1773–1787

JOURNAL OF STRUCTURAL GEOLOGY

www.elsevier.nl/locate/jstrugeo

Preliminary investigation results on fabrics and related physical properties of an anisotropic gneiss

F.J. Brosch[a,*], K. Schachner[a,1], M. Blümel[a], A. Fasching[a], H. Fritz[b]

[a]*GGG—Graz Geotechnical Group, Technical University, A-8010 Graz, Rechbauerstraße 12, Austria*
[b]*Institute of Geology and Paleontology, Graz University, A-8010 Graz, Heinrichstraße 26, Austria*

Received 25 October 1999; accepted 30 June 2000

Abstract

In order to evaluate the fabric-dependent anisotropy of a particular gneiss type, we assessed the quartz lattice and shape preferred orientations as well as the microcrack pattern statistics. In the rock mechanics laboratory, several strength and deformability tests on drilled rock samples were run and the seismic wave propagation properties along the rock's principal strain axes were determined. In the mechanical tests it turned out that despite a distinct stretching lineation with initially extreme grain elongation, the rock performs for the larger part as a transversely isotropic material with the schistosity as plane of isotropy. The anisotropy in seismic wave propagation within the plane of schistosity is attributed primarily to a highly anisotropic microcrack pattern, the distinct gneissose banding and to a lower degree to the LPO of quartz.

1. Introduction

Intact rock under near-surface boundary conditions may be considered as a system of elastic elements (minerals, components), interacting and bounded by discontinuities (grain boundaries, cleavage, microfractures/voids), and containing fluids. In fact, rock petrofabrics, especially lattice and shape preferred orientation of minerals (LPO, SPO) has been extensively investigated (Wenk, 1985; Wenk and Christie, 1991; Bunge et al., 1994) and so have petrophysics and rock anisotropy (Barla, 1974; Amadei, 1983; Montoto, 1983; Kudo et al., 1987; Crampin, 1984, 1997;). Nonetheless, the assessment of the physical anisotropy of rocks as a function of microfabrics (see the contributions to the 2nd International Congress, ISRM Belgrade, 1970; Gottschalk et al., 1990; Shea and Kronenberg, 1993; Siegesmund and Dahms, 1994; Siegesmund, 1996; Přikryl, 1998) has remained a rewarding task and several attempts from the engineering-geological and rock mechanics fields have been published (Borg and Handin, 1966; Baynes and Dearman, 1978; Hobbs et al., 1982; Cvetkovic, 1993; Ersoy and Waller, 1995; Arthur, 1996; Nasseri et al., 1997). However, a well-developed multi-directional anisotropy would call for the determination of up to 21 elastic constants just to describe the elasticity matrix of the intact material (Wittke and Sykes, 1990).

Our ongoing investigations are aimed to approach a comprehensive engineering geological characterisation of the magnitude and the directional pattern of the rock anisotropy by considering the rock fabrics and its relationship to performance in machine cutting and drilling. In this paper we use the term microfabric sensu Passchier and Trouw (1996), to describe all elements at the microscopic scale including microfractures, grain shape and arrangement, shape preferred orientation and lattice preferred orientation (texture, in a restricted sense). When not stated otherwise, all values given are mean values from a minimum of five independent determinations.

2. The rock material

2.1. General

The selected gneiss (mylonitic gneiss with porphyroclasts) crops out in highly strained regional ductile shear zones within the poly-metamorphic series of the Middle-Austroalpine nappes of the Eastern Alps, and in particular in the gneiss-dominated core complex of the Koralpe mountains (Western Styria – Carinthia/Austria, Fig. 1). These typical rock complexes are connected to their host rock series by transitional zones with prevailing lenticular and

* Corresponding author.
E-mail address: brosch@egam.tu-graz.ac.at (F.J. Brosch).
[1] Present address: Custozzagasse 5/1, 8020 Graz, Austria

0191-8141/00/$ - see front matter
PII: S0191-8141(00)00106-1

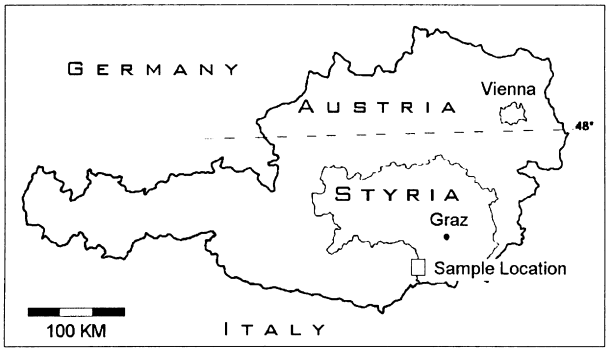

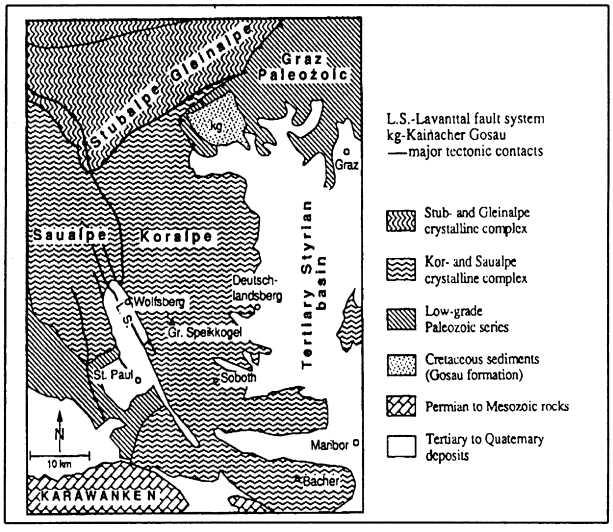

Fig. 1. The 'Koralpe' research area in Austria (modified after Gregurek et al., 1997).

augen structures. The mylonitic gneiss units experienced their major deformational and petrogenetic overprint (after a Hercynian HP event) during an Eo-Alpine eclogite facies metamorphism (100 ± 10 ma b.p., minimum $P \sim 16$ kbar, T in excess of 700°C) with subsequent northward thrusting.

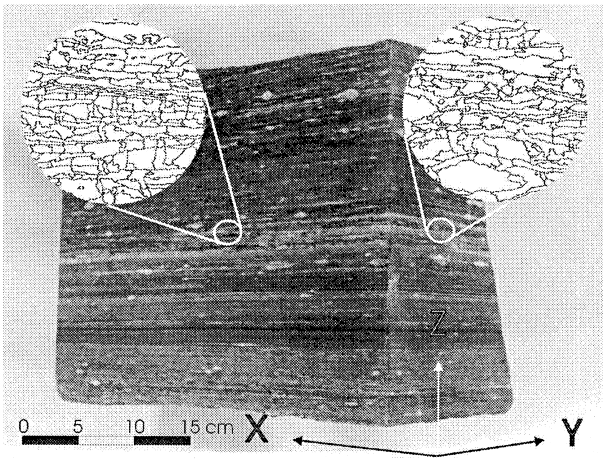

Fig. 2. Aspect of the rock, example grain fabric and structural co-ordinate system.

Table 1
Modal composition (major constituents) of 'Plattengneis' rocks as determined from X-ray diffraction

Mineral	Range (vol.%)	Mean (Std. dev.)
Quartz	34–64	47 (8.8)
Mc (mu & biot)	5–25	17 (7.2)
Plagioclase	8–19	15 (4.6)
Potassium Fsp.	1–10	5 (3.1)
Garnet (alm.)	6–14	11 (2.9)
Kyanite	< 1–8	5 (2.7)

Rapid exhumation and faulting with prevailing brittle deformation and possibly east-directed escape tectonics concluded the main tectonic evolution in the middle to upper Miocene. Details are given in Frank et al. (1983); De Roo (1983); Wimmer-Frey (1984); Krohe (1987); Beck-Managetta and Kirchmayer (1988); Ratschbacher et al. (1991); Neubauer et al. (1992); Thöny and Jagoutz (1993); Genser et al. (1996); Gregurek et al. (1997) and Kurz and Unzog (1999).

The mylonitic gneiss exhibits a distinct planar syn-metamorphic fabric which has led to some regional importance of the rock as paving/lining stone as well as in masonry (so-called "Stainzer Platten" gneiss). Macroscopically, the characteristic features of this gneiss are a near-perfect tabular fissility parallel to the tectono-metamorphic layering and mineral alignment/elongation (schistosity), and a penetrative stretching lineation, which is used as the macroscopic X-axis direction of the structural co-ordinate system (Fig. 2).

The mineral assemblage of the typical rocks may vary within the meter scale. However, slight compositional heterogeneity may be found down to the centimetre scale. Table 1 gives the range and averages of modal composition as determined from seven visually selected rock subtype samples as well as from published data (quarries NNW of Deutschlandsberg township; Platen and Höller, 1966). Accessory constituents comprise sulphidic ores, dolomite, graphite, rutile, tourmaline, apatite, zircone.

2.2. Microfabric analyses

2.2.1. General

At the microscopic scale, the mylonitic foliation and metamorphic layering are displayed by alternating polycrystal ribbons composed of quartz and feldspar (general undulatory extinction) and having a thickness of between 0.3 and 2 mm (wrapped around larger relict grains). Furthermore, the foliation is marked by mica and kyanite streaks and the elongate 'wings' of porphyroclasts: garnet and plagioclase are predominantly in-plane features with primary aspect ratios in XZ sections up to >20. The grain size of the (recrystallised) approximately equidimensional phases in both XZ and YZ sections vary between 0.03 mm and 0.9 mm, averaging 0.18 mm. Muscovite and garnet

occasionally reach a diameter of several millimeters and feldspar porphyroclasts in places may be larger than 3 cm. Most of the microfabric developed by primary ductile strain due to shear deformation and mylonitisation (expressed by grain shape and shape preferred orientation) is obliterated by dynamic grain size reduction and recrystallisation. Porphyroclasts exhibit abundant recovery (polygonisation) and recrystallisation (core–mantle and mortar) features. Quartz–quartz and quartz–feldspar grain boundaries are typically rounded-lobate and rarely serrated. Straight boundaries characterise the parent-grain outlines as well as polyphase boundaries, e.g. to mica or kyanite. Original quartz–plagioclase ribbon formation is attributed to high ductile strain and not to crack–seal processes (e.g. MacCinnon et al., 1997).

Brittle deformation phenomena at the grain scale are dominated by a distinct microcrack (MC) pattern. Virtually all the former elongated grains and porphyroclasts are cut by intra- and transgranular MC as well as intergranular (grain-boundary) microcracks (Simmons and Richter, 1976; Kranz, 1983). The MC are occasionally decorated by graphite and/or sulphide ore coatings. The general appearance of the rock in thin section showing grain and MC patterns are displayed in Fig. 3.

2.2.2. Methodical approach

Rock fabric elements have been determined both by X-ray texture goniometry for the quartz texture, and by shape preferred orientation analyses of digitised thin section line drawings (*//XZ* and *//YZ*, 6 sections each), using the Enhanced Fry and SURFOR methods of the software package STRAIN (Unzog, 1991). The mica lattice preferred orientation was not determined in detail, the thin section analysis revealed that mica flakes are concentrated in the foliation planes and are oriented almost perfectly parallel to the general schistosity (except for deviations around occasional porphyroclasts). Consequently, the planar macroscopic as well as microscopic foliation was a priori to be considered as the dominant plane of weakness in a mechanical sense and did in our opinion not deserve a specific textural (LPO) characterisation.

For a general microstructural rock characterisation the so-called 'Foliation Index' (FI, Tsidzi, 1986) and 'Texture Coefficient' (TC, Howarth and Rowlands, 1987) have been assessed. The FI considers the aspect ratio of mineral grains and their relative modal fraction. The TC index value (referring to 'texture' as a grain shape and arrangement pattern!) is a dimensionless, quantitative measure of shape, orientation and interlocking of rock constituents, aimed mainly at engineering geological purposes (for the respective evaluation formulae, see appendix).

The microcrack pattern properties were determined from line drawings of magnified thin section photographs by automated image analysis (OPTIMAS® 6.2) facilities and micro-scanline techniques, and have been evaluated with respect to the character of the cracks (like grain-boundary, intragranular-extensional, etc.), orientation, as well as with respect to the length and density of the crack traces (defect frequency and orientation analysis (DFO), Simmons et al., 1975). Only open microcracks were evaluated, traces of healed/completely mineralised MC (quartz, pyrite, dolomite) were not considered further.

When designing the procedure to investigate, in particular, the practical impacts of rock fabrics (i. e. the relationship to determined mechanical properties and to rock workability) the question arose, which scale or 'scope' of fabrics determination should appropriately be adopted. It was not clear a priori which features (microstructural or textural) and which fabric elements at which scale of observation would control the mechanical performance of the rock. The following microstructural elements are considered.

1. The inherited tectonically deformed relic grain configuration with their extreme ductile elongation and perfect parallel arrangement. This SPO dominates the macroscopic rock fabric, the locally present 'augen' structure, the compositional layering and hence the rock fissility.
2. The microfabric (LPO, SPO) of the recrystallised, predominantly equant and equidimensional quartz/feldspar grains.
3. The penetrative microcrack/microfracture system. This is related both to the relic grain shape fabric, as the fractures are best developed at right angles to the inferred tectonic stretching direction *X* (compare Vollbrecht et al., 1994) and also to the recrystallised grain fabric, since many grain boundaries are essentially microcracks.

In a first step we tentatively decided to use three categories at the lower bound of resolution ('scopes' of observation) for the microstructural analyses within the given rock microfabrics (Fig. 4). The scopes concept should serve as a tool to find the adequate scale for the investigation of the microstructure – mechanical properties interaction as follows.

1. Scope O, the scale of least resolution: domains of elongate streaks/ribbons composed of quartz–feldspar, and porphyroclasts. Considered were their outlines and boundaries.
2. Scope I, porphyroclasts and the outlines of strained, elongate parent grains, as far as their original shapes and configuration could be restored from extinction patterns, impurities, mica flakes and heterophase grain boundaries. Intergranular (grain-boundary) microcracks and transgranular cracks along high-angle subgrain boundaries were included and considered equivalent to mineral grain boundaries.
3. Scope II, representing the highest obtainable resolution of fabric elements: peculiarities of the dynamically recrystallised grain mosaique and subgrain clusters (including quartz texture), as well as the whole microcrack pattern. The latter again is considered structurally and mechanically equivalent to grain boundaries.

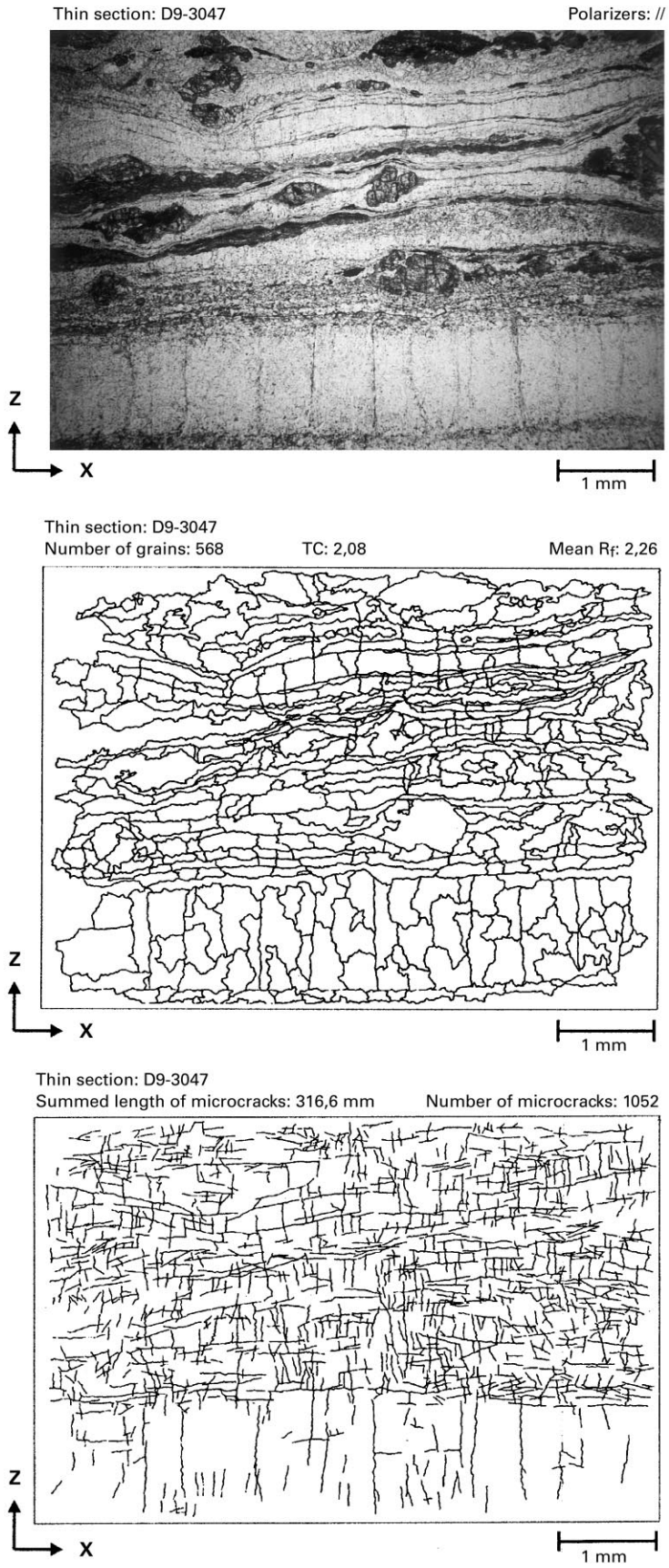

Fig. 3. Example thin section photograph, traced grain boundaries and microcrack traces pattern (thin section D9-3047).

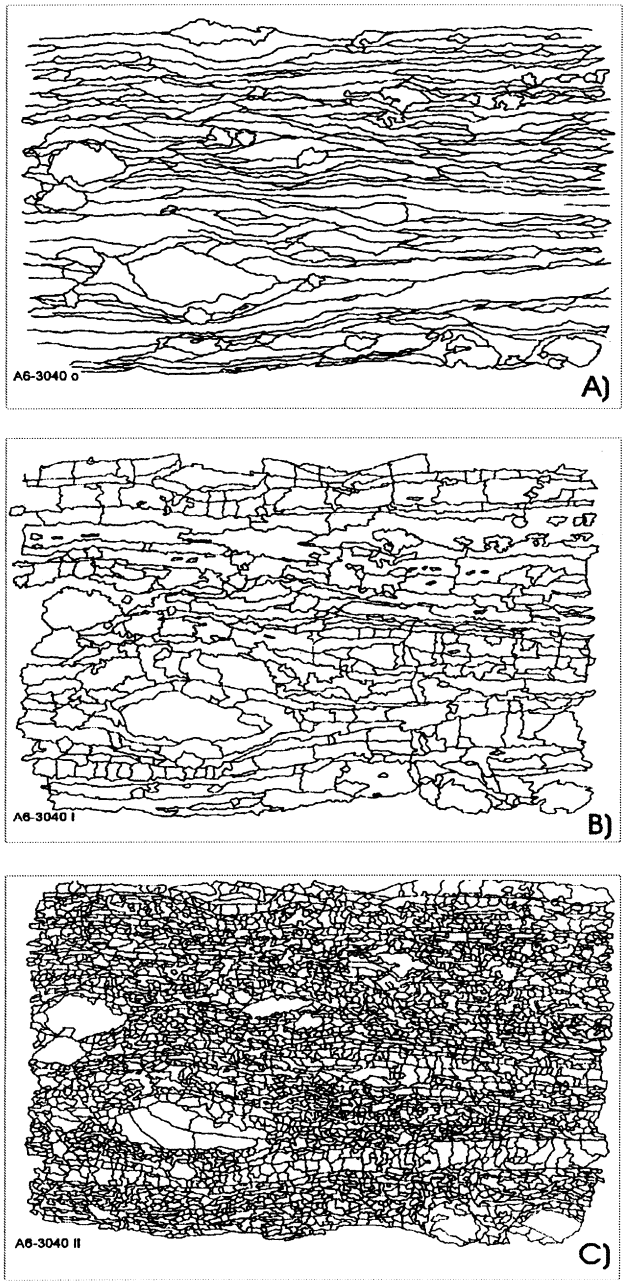

Fig. 4. Example 'scopes' of fabrics: (a) scope O: outlines of porphyroclasts and ribbons; (b) scope I: elongate parent grains, transgranular and grain-boundary microcracks; (c) scope II: recrystallised grain mosaique, subgrain boundaries and complete microcrack pattern; (thin section A6-3040*xz*).

For each section, the subfabrics related to the three scopes were carefully traced from the screen of a PETROSCOPE® thin section analyser, and/or from magnified photographs.

2.2.3. Results

The calculated axial ratio of the ellipses representing average grain shape (elongation) for the different scopes of observation differ considerably as expected. It is emphasised that in particular for scope II the calculated ellipticities and 'strain' parameters are not completely attributed to ductile strain valves, since they are based on a dynamically recrystallised grain pattern and consider the microcracks as grain boundaries. For scope 'O', the automated methods employed are not deemed to be appropriate because in many cases a closed-grain outline polygon within the area of observation (thin section) could not be established. Instead, a manual procedure was necessary to come to results for a statistically acceptable number of grains. Surprisingly, the results obtained by the (enhanced) Fry method remained contradictory.

The grain elongation assessed from scope I determinations indicate a strictly oblate shape of the strain ellipsoid (axes *X*, *Y*, *Z*) with *k* values of between 0.08 (SURFOR) and 0.20 (Enhanced Fry method): $k = (a - 1)/(b - 1)$; $a = X/Y$; $b = Y/Z$. Further calculated 'strain' parameters are given in Table 2. Note that the ellipticities (R_f) obtained from sections parallel to *YZ* exceed, in some cases, R_f of the *XZ* sections. The axis of maximum grain elongation is therefore not unambiguously established.

The quartz lattice preferred orientation (example pole diagrams in Fig. 5.) is characterised by a generally symmetrical *a*-axis pattern (poles [110] and [100] to prism planes that are minimally shifted clockwise with respect to *X*). The *c*-axis pole figures (poles to basal planes (001)) exhibit an incomplete slightly asymmetric single girdle, approximately parallel to the *YZ* plane with a general *c*-axis orientation parallel to *Y*. This configuration may be interpreted as being indicative of a prevailing high-strain deformation regime (Lister and Hobbs, 1980; Schmidt and Simpson, 1983; Schmidt and Casey, 1986; Kurz and Unzog, 1999). However, similar configurations have been described from recrystallised textures (Heidelbach et al., 2000; with references). The remarkable differences in sharpness of LPO patterns between various rock subtypes may be attributed to rock heterogeneity, to the influences of other phases (like mica) on the development of a LPO of quartz, or to strain partitioning within the thick ductile shear zone.

Due to the structural history and the distinct grain fabric of the gneiss, no random and/or isotropic MC pattern could be expected. Fig. 6 shows an example of a fracture trace configuration in the principal sections; the statistics of fracture trace numbers, length and density are given in Table 3. The following general statements can be made.

1. The MC configuration is statistically orthogonal in 3D, as can be derived from the geometry of crack traces in three mutually orthogonal thin sections per sample. The pattern is dominated by grain-boundary and cleavage cracks (set 1, parallel to the schistosity) and two sets of extensional cracks across the layering and schistosity (sets 2,3; tensile mode I cracks). Set 1 cracks are least abundant but exhibit considerable individual length.

Table 2
Calculated ellipticity (R_f), angular shear strain (γ) and angle of shear (ϕ) along two principal planes of section (X–Z, Y–Z) from the quartz grain fabrics, obtained according to the scopes O, I, II (see text) and applying two evaluation techniques

	SURFOR						Enhanced Fry					
	X–Z			Y–Z			X–Z			Y–Z		
	R_f	γ	ϕ	R_f	γ	ϕ	R_f	γ	ϕ	R_f	γ	ϕ
O	3.65	1.45	55.36	3.33	1.33	52.85	1.67	0.52	26.57	1.62	0.48	24.78
I	2.25	0.86	40.39	2.29	0.89	41.60	2.59	0.92	42.73	2.11	0.89	41.70
II	1.54	0.45	24.14	1.52	0.43	23.26	1.94	0.68	33.75	2.04	0.75	36.94

2. Both the number and length of extensional cracks are greatest parallel to the *YZ* plane (higher trace frequency in *XZ*- sections, set 2): extensional cracks are predominantly oriented at right angles to the schistosity and to the stretching lineation (*X*). Consequently, the average MC spacings for the sets differ remarkably between the principal planes of section (0.24 mm – set 2, and 0.30 mm – set 3, in *XZ* and *YZ* sections, respectively). This anisotropy may be interpreted as the result of the release of remnant stresses during exhumation (uplift-unloading) after ductile shearing in depth, in particular since one of the structural master joint sets is definitely parallel to the *YZ* plane.
3. After loading of the samples in the laboratory, both the MC summed length and frequency (inverse spacing) in the scan-lines increased considerably, however only the

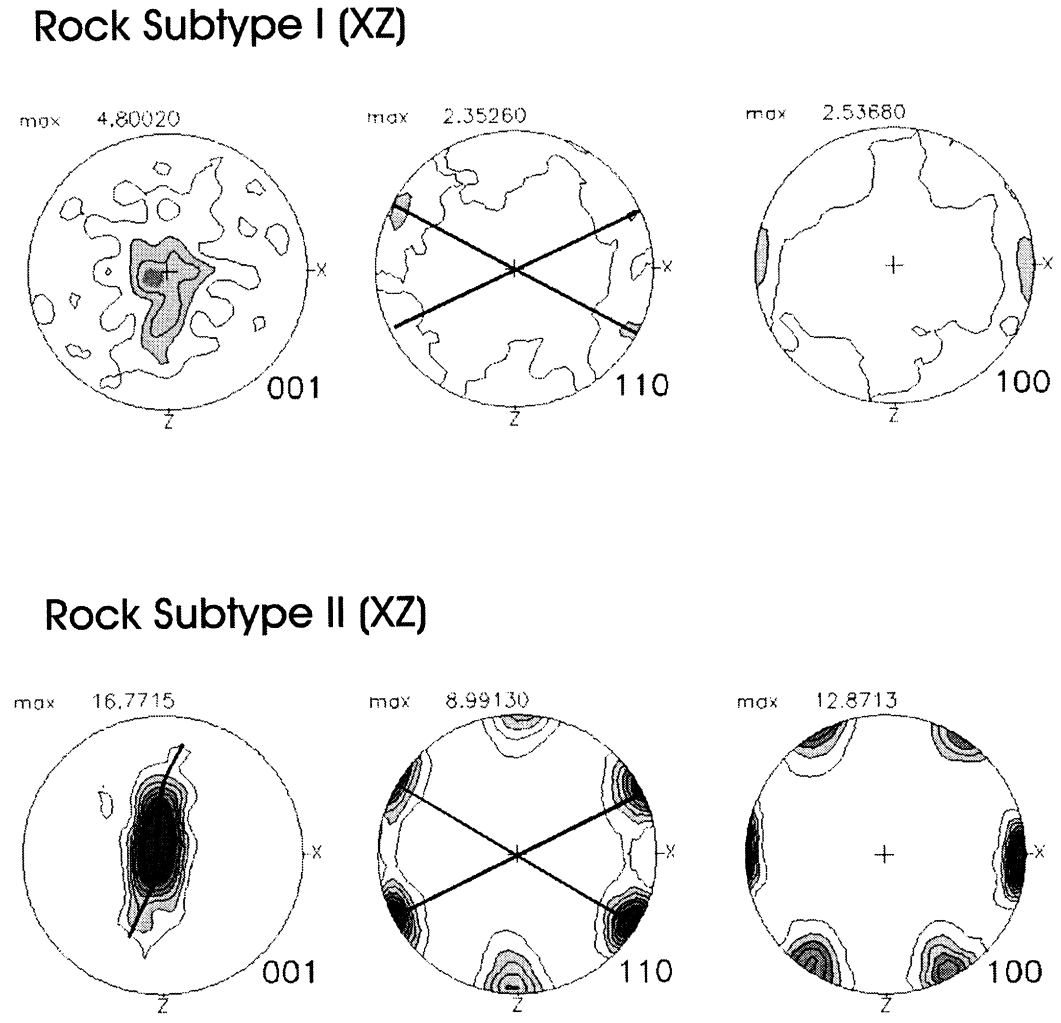

Fig. 5. Quartz crystallographic axes orientation pole figures (pole density in multiples of uniform distribution) evaluated from two extreme rock subtypes. Note that despite remarkable density differences, the type of distribution is the same.

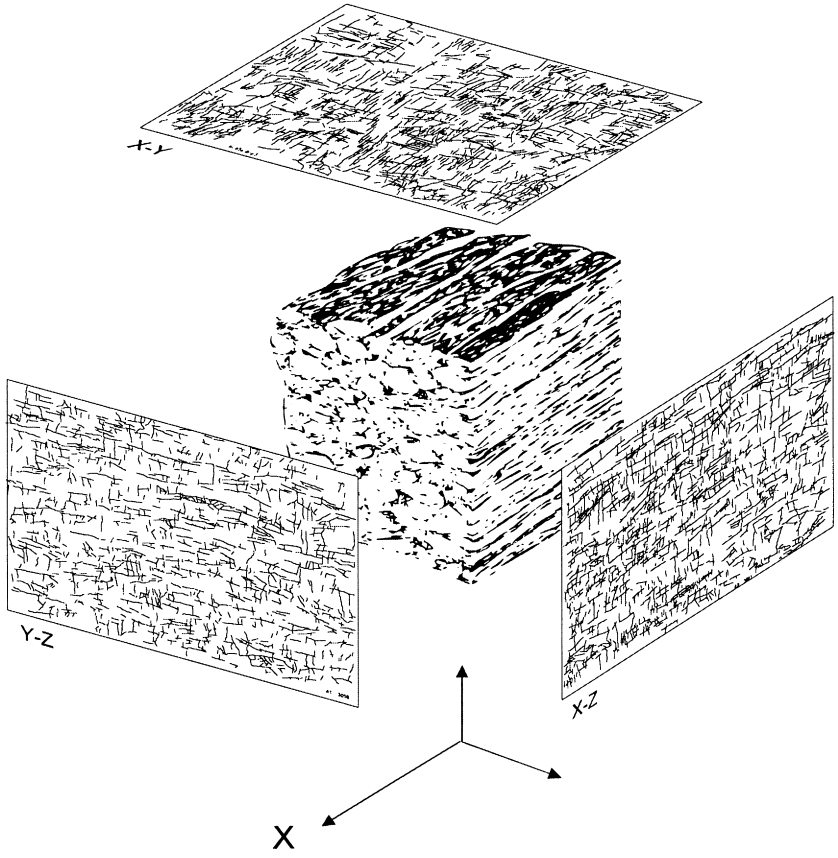

Fig. 6. Example for the statistically orthogonal microcrack-pattern as seen in the principal sections of the gneiss (thin sections A1-3036*yz*, A2-3041*xz*, D9C*xy*).

number of *YZ* cracks increased. The same effect could be observed in samples of increasing state of weathering (slightly to moderately weathered, grades II, III of Brown, 1983).

There is no significant difference in the 'texture coefficient' values that have been determined along the three principal structural axes of the rock. The slight differences between scope I (TC = 1.80 parallel to *XZ*, TC = 1.84 parallel to *YZ*) and scope II (TC = 1.70 parallel to *XZ*, TC = 1.73 parallel to *YZ*) determinations is meaningless with respect to TC-derived interpretations of rock drillability. The evaluated mean FI values for scope I (FI = 4.5) and scope II (FI = 2.52) indicate the apparently weaker developed foliation in the recrystallised fabrics due to the dominance of almost equdimensional grains. However, both proposed designations as 'moderately' and 'weakly' foliated do not represent the visual, actual rock characteristics.

3. Physical properties evaluation

3.1. Seismic investigations

3.1.1. Methodical approach

Initially, large-sized drill cores (diameter 100 mm, height >500 mm) were drilled out of one big, sound block parallel to the *X*, *Y*, and *Z* directions of the structural co-ordinate system. The velocities of ultrasonic waves (V_P, V_S) along the core axes were measured, and the following elastic parameters for the intact rock material have been calculated from the wave velocities (so-called dynamical determination): Young's modulus *E*, Poisson's ratio ν, Shear modulus *G*, Compression modulus *K*, and Lame's constant λ. The respective evaluation formulae are given in Appendix A.

In a second stage, pressures between 2 MPa and 200 MPa were applied stepwise to oriented small cylinders (diameter = 30 mm, height = 33.5 mm) in a quasi-triaxial testing procedure. Concurrently, the elastic wave velocities were measured, polarisation planes for the shear waves and their respective velocities were determined and the velocity relationship was derived (Table 5):

$$V_{S1} : V_{S2} \text{ difference } = (\{V_{S_{max}} - V_{S_{min}}\}/V_{S_{max}}) \times 100\ [\%]$$

3.1.2. Results

Table 4 summarises the measurements performed on the large cores. The values for V_p, Lame's constant λ and the Compression modulus are highest for the core drilled parallel to *Y*, that is parallel to the schistosity and at right angles to the stretching lineation. The measured elastic

Table 3
Measured quantities (mean values and Standard deviation) of the microcrack system before and after uniaxially loading and impregnating of the samples

	Number/unit area (Std. dev.)			Summed length (Std. dev.) (mm)		Spacing (Std. dev.) (mm)		
	Set 1, ~// Schistosity	Set 2 [~//*YZ*]	Set 3 [~//*XZ*]	Set 2 [~//*YZ*]	Set 3 [~//*XZ*]	Set 1[//schist.]	Set 2 [~// *YZ*]	Set 3 [~// *XZ*]
Before loading	474.00 (78.70)	690.00 (105.14)	601.33 (166.21)	347.25 (49.32)	279.03 (23.46)	0.21 (0.036)	0.24 (0.037)	0.30 (0.071)
After loading	453.00 (116.20)	939.00 (249.53)	612.62 (92.05)	462.50 (88.58)	427.21 (27.27)	0.18 (0.028)	0.16 (0.034)	0.18 (0.032)
Difference (%)	4.4	26.5	1.8	24.9	34.7	14.3	33.3	40.0

Table 4
Elastic constants as determined from ultrasonic wave propagation measurements on large bore cores drilled out along the principal structural axes (for abbreviations and parameters see text)

	V_P (m/s)	V_S (m/s)	V_P/V_S	Lamé's (kg/ms^2)	Shear mod. G (kg/ms^2)	Compression mod. K (kg/ms^2)	Poisson's ratio, ν	Young's mod. E (kg/ms^2)
Core // *X*	5750	3426	1.68	$2.734E+10$	$3.341E+10$	$4.962E+10$	0.23	$8.185E+10$
Core // *Y*	5797	3390	1.71	$3.029E+10$	$3.278E+10$	$5.214E+10$	0.24	$8.129E+10$
Core // *Z*	5000	2766	1.81	$2.782E+10$	$2.194E+10$	$4.244E+10$	0.28	$5.615E+10$
Diff. (%)	13.7	19.3	7.2	9.7	34.3	18.6	17.9	31.4

Table 5
Seismic wave propagation velocities with respect to drill core orientation and applied axisymmetric triaxial pressure (n.d.: not determined; for other abbreviations see text)

Core //X *P* (Mpa)	V_P (km/s)	V_{S1}, *X*[*XY*] (km/s)	V_{P2}, *X*[*XZ*] (km/s)	V_{P1}:V_{S2} diff. (%)
2	5.688	3.665	3.166	13.62
5	n.d.	n.d.	n.d.	n.d.
20	6.713	3.710	3.300	11.05
50	6.936	3.833	3.443	10.17
100	6.994	3.859	3.519	8.81
200	7.038	3.877	3.560	8.18
Core //*Y P* (Mpa)	V_P (km/s)	V_{S1}, *Y*[*XY*] (km/s)	V_{S2}, *Y*[*YZ*] (km/s)	V_{S1}:V_{S2} diff. (%)
2	6.145	3.565	3.282	7.94
5	6.614	3.607	3.314	8.12
20	6.912	3.706	3.367	9.15
50	7.042	3.756	3.400	9.48
100	7.056	3.828	3.449	9.90
200	7.131	3.894	3.499	10.14
Core //Z *P* (Mpa)	V_P (km/s)	V_{S1}, *Z*[*YZ*] (km/s)	V_{S2}, *Z*[*XZ*] (km/s)	V_{S1}:V_{S2} diff. (%)
2	4.978	3.271	3.178	2.84
5	5.226	2.294	3.240	1.64
20	5.259	3.337	3.268	2.07
50	5.483	3.415	3.367	1.41
100	5.621	3.464	3.429	1.01
200	5.786	3.537	3.519	0.51

wave velocities are in reasonably good agreement with the values determined from the small cores, so that we cannot see any influence of sample size ('scale effect') with the possible exception of the S-propagation velocity along the *Z* direction. The calculated Poisson's ratio values are surprisingly high as compared with the values derived from the direct laboratory tests. This might reflect a certain scale effect, but is not unusual with calculated versus measured parameters. S-split wave velocities and polarisation planes have not been determined in these tests with large drill cores.

For the small drilled samples, the P-wave velocities parallel to *Y* were again highest, while for the S-waves the split wave *X*[*XY*] (meaning: the wave propagating in the *X* direction within the *XY* polarisation plane) was initially the fastest (Table 5, Fig. 7a and b). Polarisation planes for the S-split waves turned out to coincide with the principal structural planes of the rock. The exceptional increase in the velocity ratio of shear waves along *Y* is a consequence of the generally low pressure-dependent velocity increase in the *Z* direction (Fig. 7 c). The rapid V_p increase at low pressures is associated with the progressive closure of microcracks (Meglis et al., 1996; Schild et al., 1998). In the *X* and *Y* directions, beyond a confining pressure of 50 MPa, the velocity increase was minor and the pressure dependence almost linear, which is taken as an indication for the threshold value of complete MC closure (Vernik and Zoback, 1989; Siegesmund et al., 1993; Vajdová et al., 1999). As a first approximation, this value would be achieved as a vertical stress coinciding with a depth of about 1800 m or as an induced horizontal stress ($\rho \approx 2.7$ g/cm^2, $\nu \approx 0.3$) at approx. 4400 m below the surface (Hoek and Brown, 1980).

Lowest velocities were obtained in all directions containing the *Z*-axis, and V_p parallel to *Z* increased steadily up to a confining pressure of 200 MPa (Fig. 7a). This is attributed mainly to the attenuation effect (compressibility) of mica layers with parallel-oriented cleavage cracks between the quartz–feldspar ribbons.

3.2. Rock mechanics tests

3.2.1. Methodical approach

Series of cores (diameter = 50 mm, height–diameter ratio ≥ 2) were drilled out of a visually intact, homogeneous block of rock in 30° intervals along the principal planes of the macroscopic structural co-ordinate system (Fig. 8).

For uniaxial compressive and (quasi-) triaxial tests, a servo-hydraulic testing system was used (MTS Minneapolis, USA, both constant incremental stress rate and constant strain mode options, closed-loop controlling). Poisson's ratio was calculated using each specimen's circumferential dilative strain versus the axial compressive strain; therefore this is an integration of transversal strains along the relevant axes with respect to the longitudinal strain. The determination of Young's modulus is not uniquely defined in international rock mechanics standards. For this study we used the average modulus of the linear proportion of the axial stress/strain curve. Two complete test suites have been performed to date and the given values are simple averages.

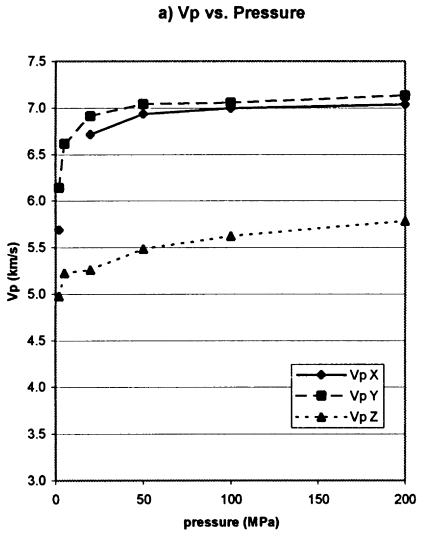

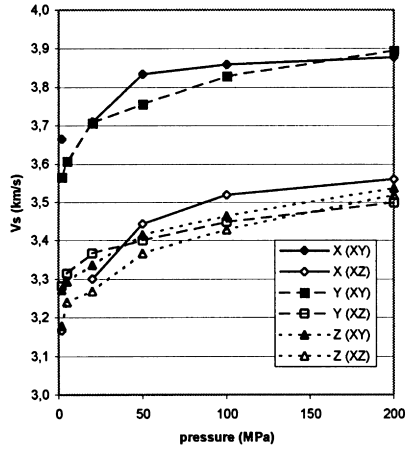

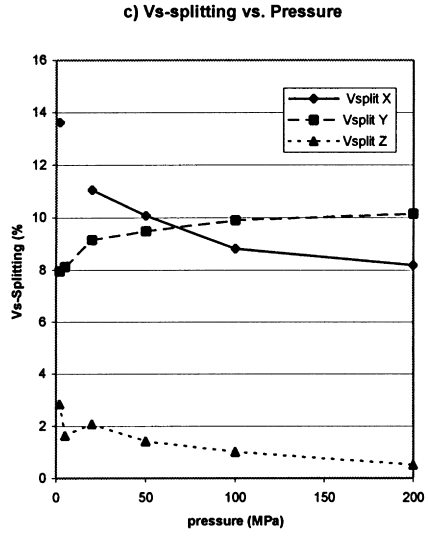

Fig. 7. (a)–(c) Pressure-dependent seismic wave velocities along the principal directions of the rock as determined from small drill cores. In (b), the designation: *X*(*XZ*) etc. denotes the S-wave travelling in direction *X* within the polarisation plane *XZ*. In (c), the velocity difference (%) for any two S-split waves according to propagation direction and confining pressure are given.

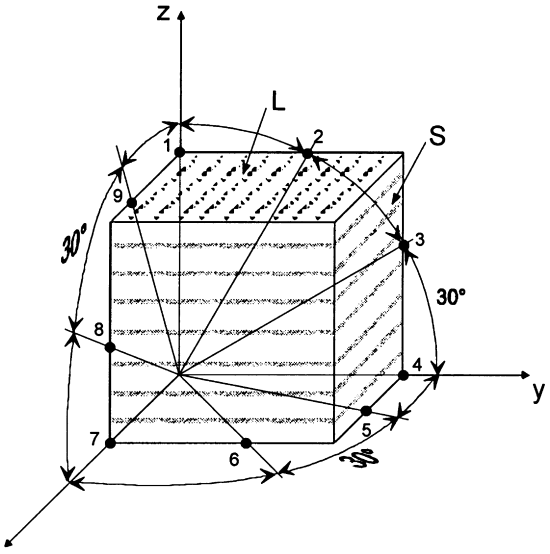

Fig. 8. Sketch of tested rock specimen with drilled sample orientations (1…9) in relation to schistosity (*S*), stretching lineation (*L*) and structural axes (*X,Y,Z*).

A second set of drilled samples was prepared in order to track the MC development and microscopic rock destruction patterns under laboratory test loading conditions. The cores were uniaxially loaded up to, and above their peak strength and consequently vacuum-impregnated (decorated) by dye-coloured resin. The visually enhanced microcrack pattern was evaluated optically and with image analysis facilities by comparing it with the original MC pattern characteristics of a reference sample from the same specimen.

Rock tensile strength was calculated and tested indirectly by Brazilian testing (line-load application along the long side of drilled rock cylinders, performed for the three principal structural co-ordinate axes only) and by a modified line-load testing procedure: Two cylindrical steel rods (diameter = 9 mm) between load platens were used to induce a tensile stress within 8-mm-thick cut and ground core discs (average grain size < 0.4 mm) without porphyroclasts or visible healed cracks within the plane of the applied load, which had been inserted between the rods (Fig. 9; 'Nadelversuch': Paulmann, 1966). The direction of this line-load application was changed in 30° intervals in succession with respect to the schistosity trace and the stretching lineation, respectively. The values obtained from these tests are not yet statistically correlated to direct tensile strength and are considered as index values only.

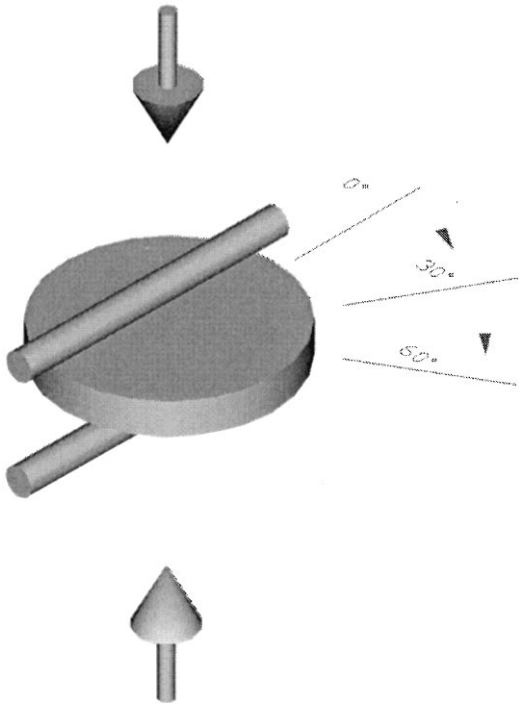

Fig. 9. Sketch of the line loading system for drill core disks in an adapted Point Load tester; large arrows indicate load application direction; angle designations symbolise the five load application directions (0–150°) in steps of 30° with respect to a reference direction (trace of schistosity or stretching lineation) on each sample.

3.2.2. Results

Fig. 10 seems to indicate that the determined elastic parameters describe a transversely isotropic material with the schistosity (*XY*) as the plane of isotropy. It is well-known that for foliated rocks, the uniaxial (unconfined) compressive strength (UCS in Fig. 10) is highest in the loading direction normal to the schistosity planes (*Z*) and lowest at acute angles to these planes (directions '3', '8' in Fig. 10). The strength anisotropy along the principal structural axes (*Z* vs. (*X,Y*)) is 13%, the maximum difference (*Z* vs. '3') is 62%. The anisotropy of Young's modulus reaches 36% between its highest level parallel to the schistosity planes (directions '4' through '7') and the minimum value in the *Z* direction, as it is commonly observed. Poisson's ratio values for the specimens tested at acute angles to the *Y* axis (and parallel to *Y*) as well as parallel to *X* are noticeably high (Fig. 10c). These results may at least qualitatively reflect the role of the existing (and, probably during the loading procedure, concurrently developing) MC geometry and abundance pattern, as well as the influence of the schistosity (opening of the load-parallel cracks in the *YZ* and *XZ* planes). However, with only two tests series performed until now, a statement regarding the elastic anisotropy pattern in 3D may not yet be justified.

The modified line-load tests rendered a more complex result (Fig. 10d). Index 'tensile' strength is significantly lowest parallel to *Z*, that is normal to the schistosity. In the *YZ* plane the highest 'tensile' strength was achieved (even in moderately weathered samples; four tests) at 15–30° off the *Y* axis. For the *XY* plane, the relatively lowest 'tensile' strength values are obtained in the direction *X*. From this orientation the apparent tensile strength increased steadily to a relative maximum, approximately 15–30° off *Y*.

This latter behaviour may be tentatively explained by the geometric fact that the minimum encountered fracture frequency for an orthorhombic fracture system with different set frequencies is at acute angles to the higher-frequency set (Priest, 1993).

The Brazilian tests revealed a statistically almost transversely isotropic pattern for the indirect tensile strength (Table 6). However, the strength parallel to *Y* in three out of four tests is slightly higher than in the *X* direction. These somewhat ambiguous and not significantly MC-bound strength patterns could result from a certain reinforcement action of the mica streaks, which are predominately aligned along *X* within the plane of schistosity.

With the inspection of the MC configuration after loading it turned out that fractures parallel to *XZ* had increased by almost 35% in summed length (predominantly by coalescence). The *YZ* cracks (normal to *X*) had increased by about 25% in summed length, but had increased considerably in number (Table 3).

4. Discussion and conclusions

The preliminary results of ongoing studies for the relationship between microstructural fabrics and physical/mechanical properties of the 'Stainzer Platten' gneiss may be summarised as follows.

1. The dominant macroscopic stretching lineation and ductile parent-grain elongation of the gneiss is neither sufficiently represented in the SPO and MC subfabrics, nor with respect to the rock mechanics deformation and strength pattern (UCS, elastic parameters). Apparently, the recrystallised grain and microcrack subfabrics (scope II) are responsible for the mechanical properties, except for the macroscopic fissility, which is a consequence of the scopes O–I microstructures.
2. Seismic wave velocities obtained from the small cores rendered a marked anisotropic behaviour (including S-wave splitting) in close relation to the structural coordinates. The high V_p values measured in the *Y* direction are attributed to both the distinct quartz (and mica?) LPO and to a separation effect along *YZ*-planes of the brittle-deformation microfabrics. Qualitatively, the same results have been obtained from the large cores, a significant dependence on the scale effect was not observed.
3. TC is not thought to be an appropriate measure of rock fabrics and derived physical properties, because it does not consider grain size and microcracks. Moreover, the 'Form' and 'Angle' factors in TC are mutually interdependent

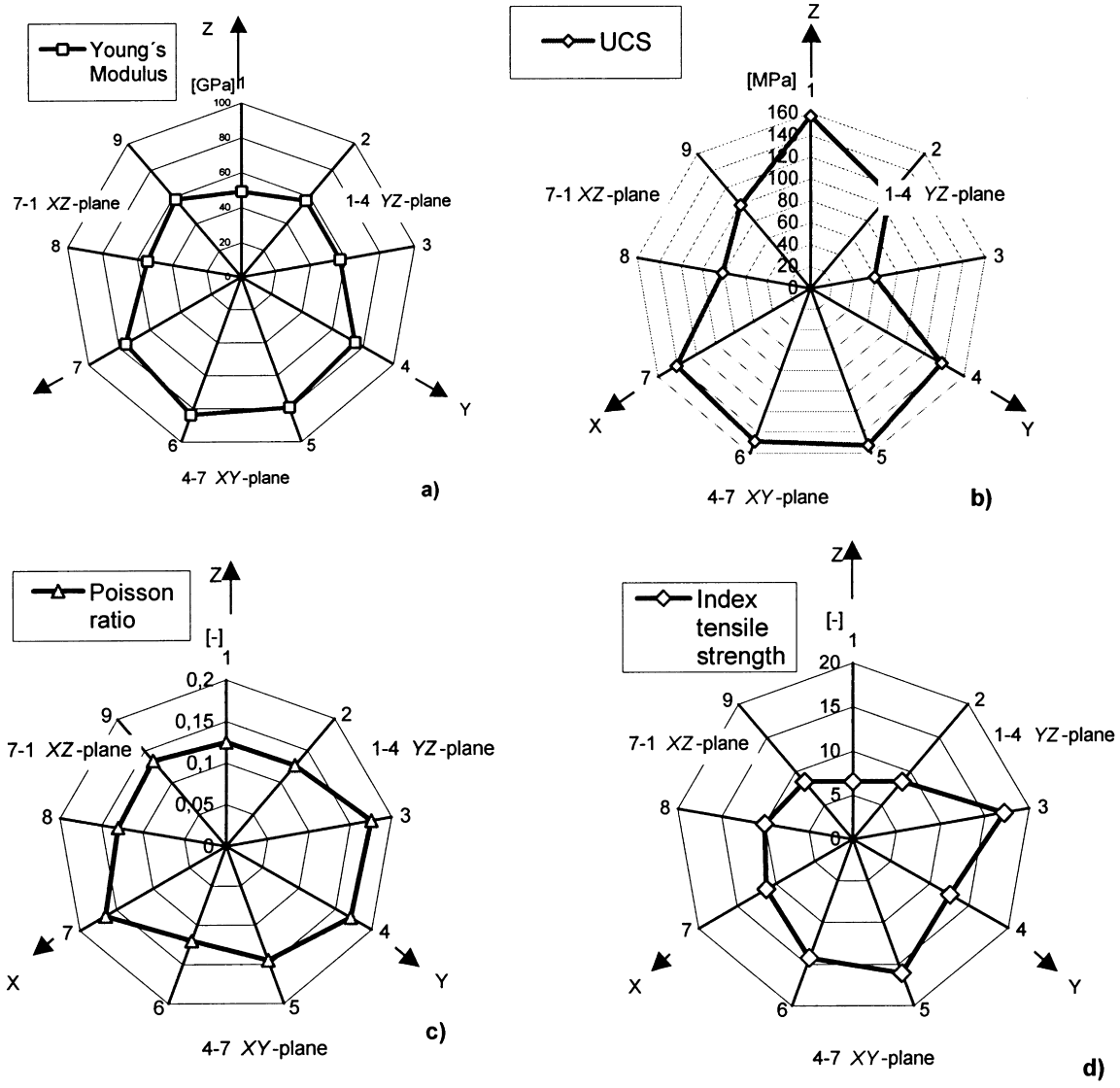

Fig. 10. a–d: Strength values and elastic parameters as determined along the principal sections in directions 1…9 of Fig. 8 (UCS = uniaxial compressive strength).

Table 6
Tensile strength along the principal tectonic axes as determined by Brazilian tests

	σ_t in direction		
	//X	//Y	//Z
Brazilian test values (MPa)	12.93	11.13	8.67
	14.51	14.99	6.19
	15.57	15.60	6.74
	20.05	20.44	9.00
Mean	15.8	15.5	7.6
(Std. dev.)	(2.64)	(3.30)	(1.20)

(c.f. Azzoni et al., 1996). FI on the other hand, lacks grain interlocking and phase concentration parameters. For geotechnical characterisation purposes it may be sufficient to use the Mica Fabric Index, ('Glimmer–Gefüge-Index': Büchi, 1984) as a very simple measure for the SPO and distribution concentration of mica and hence for the gneissosity and fissility.

4. The most abundant short *YZ* microcracks across the quartz–feldspar ribbons have a measurable influence on loading strains (Poisson's ratio). Owing to microcrack anisotropy, both Brazilian indirect tensile strength and modified line load strength tests indicate a distinct (but not yet statistically significant) difference in the tensile strength values along the *X* and *Y* axes, respectively. A slight scale effect could be responsible for the high Poisson's ratios determined (dynamically) for the large cores as compared with the rock mechanics tests.

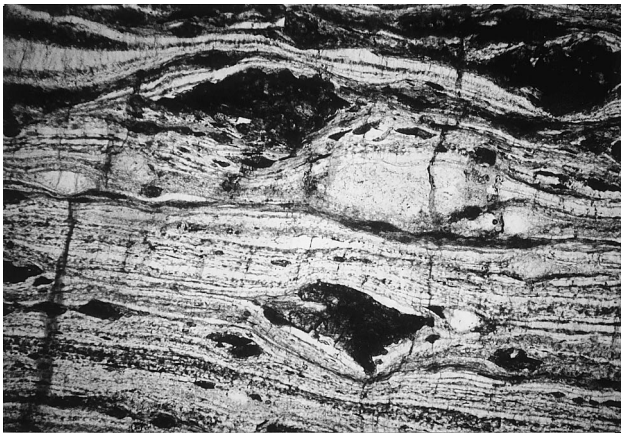

Fig. 11. Example for the pre-failure coalescence of *YZ*-microcracks (dark, offsetting approx. NNE–SSW, besides faint narrow-spaced cracks across the layering), eventually leading to macroscopic failure planes (thin section B7/2*xz*).

5. Plastic strain and eventual failure of the specimens tested in axial compression occurred predominantly by the opening of existing extensional cracks (and associated shear in cleavage cracks of mica layers) and by their coalescence (Lockner and Moore, 1992). The formation of new mode-I cracks within quartz–feldspar layers seemed to be a subordinate process (Fig. 11). The observed anisotropic increase of microcracks (greater in length parallel to *XZ* and more small cracks parallel to *YZ*) during the loading tests, and hence the resulting statistically isotropic spacing values (0.16–0.18 mm), may point to a tendency of smoothing out the initial mechanical rock anisotropy due to microcrack development.

Acknowledgements

The authors thank DMT GmbH Essen/FRG and IGDL-Univ. Goettingen/FRG (Prof. S. Siegesmund) for performing the seismic investigations on drill cores, Prof. G. Riedmüller (GGG) for financial aid and T. Button (GGG) for his advice concerning the English. In particular we acknowledge the support by Prof. M. Montoto (Univ. Oviedo/E), H. Dürrast and B. Leiss (IGDL-Univ. Goettingen/FRG) as well as an anonymous referee. Their thorough review and constructive comments considerably helped to improve the contents and presentation of this paper.

Appendix A

The TC (Howarth and Rowlands, 1986) is determined as:

$$\mathrm{TC} = \mathrm{AW}\left[\left(\frac{N_0}{N_0 + N_1} \times \frac{1}{\mathrm{FF}_0}\right) + \left(\frac{N_1}{N_0 + N_1} \times \mathrm{AR}_1 \times \mathrm{AF}_1\right)\right] \tag{A1}$$

Where AW is the weighting factor for grain packing density, like in sedimentary rocks (for metamorphic rock AW = 1); N_0 is the number of grains with aspect ratio <2.0; and N_1 is the number of grains with aspect ratio >2.

FF_0 is the mean of the form factors (FF) of all grains with aspect ratio <2.0; FF describes the deviation of grains from a circular outline (FF = 1) and the 'roughness' of grain boundaries, respectively:

$$\mathrm{FF} = \frac{4\pi \times (\text{area})}{(\text{perimeter})^2} \text{ for each grain.} \tag{A2}$$

AR_1 is the mean of all aspect ratios >2.

AF_1 is the angle factor, a measure for the shape preferred orientation of grains ($\mathrm{AF}_1 =$ AF/5; $0.2 \preceq \mathrm{AF}_1 \preceq 1$). For the determination of AF, the angular differences of Feret's maximum diameter between each and any grains are grouped into nine classes of ten degrees each (0–10, 10–20, etc.); accordingly, nine weighting factors (1…9) are attributed to the classes:

$$\mathrm{AF} = \sum_{i=1}^{9}\left[\frac{x_i}{\frac{N_1 \times (N_1 - 1)}{2}}\right] \times i \tag{A3}$$

X_i is the number of measurements (angular differences) within each class, and i is the weighting factor of the respective class.

The FI (Tsidzi, 1986) is to be evaluated from the sections with the largest aspect ratios (parallel to *XZ)* and is defined as:

$$\mathrm{FI} = \frac{1}{100} \times \sum_{1}^{n} M_i \times S_i \tag{A4}$$

M_i is the modal fraction (%) of the respective mineral component and S_i is the mean of all aspect ratios of the respective minerals.

The formulae used for the evaluation of rock elastic parameters from seismic wave velocities are (the common relationships for use in mechanical laboratory testing are given in brackets):

Young's modulus E (stress–strain ratio: σ/ε):

$$E = 2V_S^2 \times \rho \times (1 + \nu) \tag{A5}$$

Poisson's ratio ν (strain ratio: $-\Delta\varepsilon_{\text{lateral}}/\Delta\varepsilon_{\text{axial}}$):

$$\nu = \left(V_S^2 - \frac{V_P^2}{2}\right) \Big/ \left(V_S^2 - V_P^2\right) \tag{A6}$$

Shear modulus G ($E/2[1 + \nu]$):

$$G = \rho \times V_S^2 \tag{A7}$$

Compression (Bulk) modulus K ($E/3[1-2\nu]$):

$$K = \rho \times V_P^2 - \frac{4G}{3} = \lambda + \frac{2G}{3} \tag{A8}$$

Lame's constant λ ($E\nu/[1+\nu]\times[1-2\nu]$):

$$\lambda = \rho \times \left(V_P^2 - 2V_S^2\right) \quad \text{(A9)}$$

Where V_P, V_S are the compressional and shear wave velocities, respectively, ρ is the unit weight (2.85 g/cm^3).

References

Amadei, B., 1983. Rock Anisotropy and the Theory of Stress Measurements. Springer, Berlin.

Arthur, C.D., 1996. The determination of rock material properties to predict the performance of machine excavation in tunnels. Quarterly Journal of Engineering Geology 29, 67–81.

Azzoni, A., Bailo, F., Rondena, E., Zaninetti, A., 1996. Assessment of texture coefficient for different rock types and correlation with uniaxial compressive strength and rock weathering. Rock Mechanics and Rock Engineering 29/1, 39–46.

Barla, G., 1974. Rock anisotropy; theory and laboratory testing. International Centre for Mechanical Sciences, Courses & Lectures 165, 131–169.

Baynes, F.J., Dearman, W.R., 1978. The relationship between the microfabric and the engineering properties of weathered granite. Bulletin IAEG 18, 191–197.

Beck-Managetta, P., Kirchmayer, M., 1988. Die Quarz-, Glimmer- und Feldspatkorngefüge in den acht Plattengneiskomplexen der Koralpe. Jahrbuch der Geoogischen Bundesanstalt, 131/4, pp. 505–532.

Borg, I, Handin, J., 1966. Experimental deformation of crystalline rocks. Tectonophysics 3, 249–368.

Brown, E.T., 1983. Rock characterization testing and monitoring—ISRM suggested methods. Pergamon Press, Oxford.

Bunge, H.J., Siegesmund, S., Skrotzki, W., Weber, K., 1994. Textures of Geological Materials. DGM Informationsgesellschaft, Oberursel.

Büchi, E., 1984. Einfluß geologischer Parameter auf die Vortriebsleistung einer Tunnelbohrmaschine, mit besonderer Berücksichtigung der Gesteinsanisotropie—Inauguraldissertation Phil.—Naturwiss. Fak. Universität Bern.

Crampin, S., 1984. Effective anisotropic elastic constants for wave propagation through cracked solids. Geophysical Research of the Royal Astronomical Society 76, 135–145.

Crampin, S., 1997. Going APE I: Modeling the inherent anisotropy of intact rock.—Expanded abstracts. SEG International Exposition & 67th Annual Meeting, Dallas.

Cvetkovic, M.S., 1993. Static and dynamic properties of gneiss as a function of foliation. Proceedings of the International Symposium Geotechnical Engineering of hard soils—soft rocks, Athens/Greece, Balkema, Rotterdam, pp. 63–69.

De Roo, J.A., 1983. A structural section through the Plattengneis mylonites of the Koralpe, Austria. Thesis, Institute for Earth Sciences, University of Utrecht/NL.

Ersoy, A., Waller, M.D., 1995. Textural characterisation of rocks. Engineering Geology 39, 123–136.

Frank, W., Esterlus, M., Frey, M., Jung, G, Krohe, A., Weber, J., 1983. Die Entwicklungsgeschichtevon Stub- und Koralpenkristallin und die Beziehung zum Grazer Paläozoikum—Jahresbericht 1982, Hochschulschwerpunkt S15: Die frühalpine Geschichte der Ostalpen 3, 263–293, Wien.

Genser, J., VanWees, J.D., Cloetingh, S., Neubauer, F., 1996. Eastern Alpine tectono-metamorphic evolution—constraints from 2-dimensional P–T–t modeling. Tectonics 15, 584–604.

Gottschalk, R., Kronenberg, A.K., Russel, J.E., Handin, J., 1990. Mechanical anisotropy of gneiss: Failure criterion and textural sources of directional behaviour. Journal of Geophysical Research 95/B13, 613–634.

Gregurek, D., Abart, R., Hoinkes, G., 1997. Contrasting eoalpine P–T evolutions in the southern Koralpe, Eastern Alps. Mineralogy and Petrology 60, 61–80.

Heidelbach, F., Kunze, K., Wenk, H.-R., 2000. Texture analysis of a recrystallized quartzite using electron diffraction in the scanning electron microscope. Journal of Structural Geology 22/1, 91–105.

Hobbs, B.E., Means, W.D., Williams, P.F., 1982. The relationship between foliation and strain: an experimental investigation. Journal of Structural Geology 4 (4), 411–428.

Hoek, E., Brown, E.T., 1980. Underground Excavations in Rock. The Institute of Mining and Metallurgy, London.

Howarth, D.F., Rowlands, J.C., 1987. Quantitative assessment of rock texture and correlation with drillability and strength properties. Rock Mechanics and Rock Engineering 20, 57–85.

Kranz, R.L., 1983. Microcracks in rocks: a review. Tectonophysics 100, 449–480.

Krohe, A., 1987. Kinematics of Cretacous nappe tectonics in the Austroalpine basement of the Koralpe region (eastern Austria). Tectonophysics 136, 171–196.

Kudo, Y., Hashimoto, K.-I., Sano, O., Nakagawa, K., 1987. Relation between physical anisotropy and microstructure of granitic rocks in Japan. Proceedings of the 6th International Congress ISRM Montreal, Balkema, Rotterdam, pp. 429–432.

Kurz, W., Unzog, W., 1999. Variation of quartz textures within the Plattengneiss of the Koralm Complex (Eastern Alps). Mitteilungen Naturwissenschaftlicher Verein Steiermark 129, 33–45.

Lister, G.S., Hobbs, B.E., 1980. The simulation of fabric development during plastic deformation and its application to quartzite: the influence of deformation history. Journal of Structural Geology 2, 355–370.

Lockner, D.A., Moore, D.E., 1992. Microcrack interaction leading to shear fracture. Proceedings of the 33rd U.S. Symposium on Rock Mechanics, Santa Fe/New Mexico. Balkema, Rotterdam, pp. 807–815.

MacCinnon, P., Fueten, F., Robin, P.-Y.F., 1997. A fracture model for quartz ribbons in straight gneisses. Journal of Structural Geology 19/1, 1–14.

Meglis, I.L., Greenfield, R.J., Engelder, T., Graham, E.K., 1996. Pressure dependence of velocity and attenuation and its relationship to crack closure in crystalline rocks. Journal of Geophysical Research 10/B8, 17523–17533.

Montoto, M, 1983. Petrophysics: the petrographic interpretation of the physical properties of rocks. Proceedings of the 5th International Congress ISRM Melbourne. Balkema, Rotterdam, pp. B93–B98.

Nasseri, M.H., Rao, K.S., Ramamurthy, T., 1997. Failure mechanisms in schistose rocks, International Journal of Rock Mechanics and Mining Science 34, paper 219.

Neubauer, F., Genser, J., Fritz, H., Wallbrecher, E., 1992. Alpine Kinematics of the Eastern Central Alps. ALCAPA Field guide (IGP/KFU Graz), pp. 127–136.

Paulmann, H.G., 1966. Messungen der Festigkeits-Anisotropie tektonischen Ursprungs an Gesteinsproben. Proc. 1st International Congress ISRM, Lisboa 1996, Theme .6 2, 125–131.

Passchier, C.W., Trouw, R.A.J., 1996. Microtectonics. Springer, Berlin, Heidelberg, New York.

Platen, H.V., Höller, H., 1966. Experimentelle Anatexis des Stainzer Plattengneises von der Koralpe, Steiermark, bei 2, 4, 7 und 10 kb H_2O-Druck. Neues Jahrbuch für Mineralogie Abhandlungen 106/1, 106–130.

Priest, S.D., 1993. Discontinuity Analysis for Rock Engineering. Chapman & Hall, London.

Prikryl, R., 1998. The effect of rock fabric on some mechanical properties of rocks: an example of granites.—Doctoral Thesis, Inst. Geochemistry, Mineralogy and Mineral Resources, Faculty of Science, Charles University, Prague.

Ratschbacher, L., Frisch, W., Linzer, H.-G., 1991. Lateral extrusion in the eastern alps, part II: structural analysis. Tectonics 10, 257–271.

Schild, M., Vollbrecht, A., Siegesmund, S., Reutel, C., 1998. Microcracks

in granite cores from the EPS-1 geothermal drill hole, Soultz-sous-forêts (France): paleostress directions, paleofluids and crack-related V_P-anisotropies. Geologische Rundschau 86, 775–785.

Schmidt, S.M., Simpson, C., 1983. The evaluation of criteria to deduce the movements in sheared rocks. Bulletin of the Geological Society of America 94, 1281–1288.

Schmidt, S.M., Casey, M., 1986. Complete fabric analysis of some commonly observed quartz *c*-axis patterns. Geophysical Monographs 36, 263–286.

Shea, W.T., Kronenberg, A.K., 1993. Strength and anisotropy of foliated rocks with varied mica contents. Journal of Structural Geology 15 (9–10), 1097–1121.

Siegesmund, S., Vollbrecht, A., Pros, Z., 1993. Fabric changes and their influence on P-wave velocity patterns: examples from a polyphase deformed orthogneiss. Tectonophysics 225, 477–492.

Siegesmund, S., Dahms, M., 1994. Fabric-controlled anisotropy of elastic, magnetic, and thermal properties of rocks. In: Bunge, H.J., Siegesmund, S., Skrotzki, W., Weber, K. (Eds.), Textures of Geological Materials, DGM Informationsgesellschaft Verlag, Oberursel, pp. 353–381.

Siegesmund, S., 1996. The significance of rock fabrics for the geological interpretation fo geophysical anisotropies. Geotektonische Forschungen 85, 1–123.

Simmons, G., Todd, G., Baldridge, W.S., 1975. Toward a quantitative relationship between elastic properties and cracks in low porosity rocks. American Journal of Science 275, 318–345.

Simmons, G., Richter, D., 1976. Microcracks in rock. In: Strens, R.G.J. (Ed.), The Physics and Chemistry of Minerals and Rocks, Wiley & Sons, London.

Thöny, M., Jagoutz, E., 1993. Isotopic constraints for the eo-Alpine high-P metamorphism in the Austroalpine nappes of the Eastern Alps: bearing on Alpine Orogenesis. Schweizerische Mineralogische und Petrographische Mitteilungen 73, 177–189.

Tsidzi, K.E.N., 1986. A quantitative petrofabric characterisation of metamorphic rocks. Bulletin IAEG 33, 2–12.

Unzog, W., 1991. Contrasting results of strain analysis from different rocks with various methods. Terra Abstracts 5/3, 40.

Vajdová, V., Přikryl, R., Proš, Z., Klíma, K., 1999. The effect of rock fabric on P-wave velocity distribution in amphibolites. Physics of the Earth and Planetary Interiors 114, 39–47.

Vernik, L., Zoback, M.D., 1989. Elastic and strength anisotropy of cores from the Cajon Pass scientific drill hole: Effects on seismic wave propagation and stress-induced wellbore breakouts. EOS Transactions 70, 479.

Vollbrecht, A., Olesen, N.O., Schmidt, N.H., Weber, K., 1994. Crystallographic microcrack orientation in quartz from a granite—a combined ECP/U-stage study. Textures of Geological Materials, DGM Informationsgesellschaft-Verlag, Oberursel, pp. 345–352.

Wenk, H.R., 1985. Preferred Orientation in Deformed Metals and Rocks: An Introduction to Modern Texture Analysis. Academic Press, Orlande.

Wenk, H.-R., Christie, J.M., 1991. Comments on the interpretation of deformation textures in rocks. Journal of Structural Geology 13, 1091–1110.

Wimmer-Frey, I., 1984. Gefüge- und Metamorphoseuntersuchungen am Plattengneis der zentralen Koralm, W-Steiermark.—Doctoral Thesis (unpublished), University of Vienna.

Wittke, W., Sykes, R., 1990. Rock Mechanics: Theory and Applications with Case Histories. Springer, New York.